JCTC Journal of Chemical Theory and Computation

pubs.acs.org/JCTC Article

Error-Mitigation Enabled Multicomponent Quantum Simulations beyond the Born−Oppenheimer Approximation

Delmar G. A Cabral, Brandon Allen, Fabijan Pavošević, Sharon Hammes-Schiffer, Pablo Díez-Valle, Jack S. Baker, Gaurav Saxena, Thi Ha Kyaw,* and Victor S. Batista*

Cite This: J. Chem. Theory Comput. 2026, 22, 1760−1769 Read Online

ACCESS | Metrics & More | Article Recommendations

ABSTRACT: We introduce a multicomponent unitary coupled cluster (mcUCC) framework for quantum simulations of molecular systems that incorporate both electronic and nuclear quantum effects beyond the Born−Oppenheimer approximation. Using the nuclear−electronic orbital formalism, we construct mcUCC ansätze for positronium hydride and molecular hydrogen with a quantum proton, and analyze hardware requirements for different excitation truncations. To further reduce resource costs effectively, we employ the local unitary cluster Jastrow ansatz and implement it experimentally on IBM Q's Heron superconducting hardware. With the Physics-Inspired Extrapolation error mitigation protocol, the computed ground-state energies remain within chemical accuracy, consistent with the stated uncertainty level. These results provide the first demonstration of error-mitigated multicomponent correlated simulations on quantum hardware and outline a path toward scalable algorithms unifying electronic and nuclear degrees of freedom.

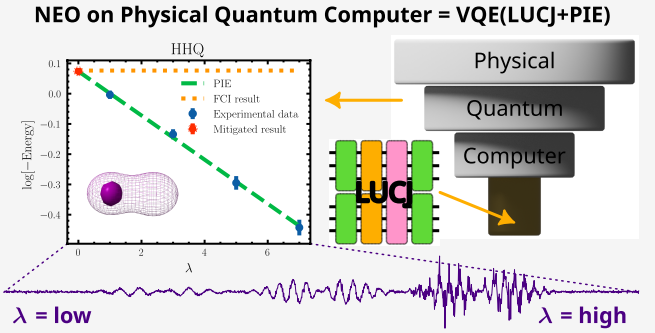

Downloaded via YALE UNIV on March 16, 2026 at 20:35:00 (UTC).
See https://pubs.acs.org/sharingguidelines for options on how to legitimately share published articles.

1. INTRODUCTION

Many fundamental chemical processes involve nuclear quantum effects that challenge the Born−Oppenheimer (BO) separation of electronic and nuclear motion. Nuclear quantum effects, such as zero-point energy, nuclear delocalization, and tunneling, have been shown to be important in a wide range of chemical and biological systems.[1−4] Phenomena such as proton tunneling, hydrogen transfer, and proton-coupled electron transfer are governed by zero-point motion and nonadiabatic couplings that significantly influence reaction thermodynamics and kinetics.[5−8] Classical treatments that confine nuclei to point particles can therefore produce qualitatively incorrect predictions.

The nuclear−electronic orbital (NEO) framework addresses this limitation by treating selected light nuclei (typically protons) quantum mechanically alongside electrons. By incorporating nuclear delocalization, tunneling, and electron−nucleus correlation directly into the wave function, NEO theory provides a unified and systematically improvable approach for systems in which electronic and nuclear degrees of freedom are strongly coupled.[9,10] A wide range of NEO density functional theory[11−14] and wave function methods,[15−19] such as coupled-cluster theory and configuration interaction theory, have been developed and applied to molecular systems.

Despite the accuracy of NEO-based methods, solving correlated electronic−nuclear structure problems remains computationally demanding. Classical algorithms for exact solutions scale exponentially with system size, motivating the use of quantum computation as an alternative route to scalable molecular simulation.[20,21] Two major paradigms have emerged: quantum phase estimation (QPE) and the variational quantum eigensolver (VQE).[22−24] QPE can, in principle, yield exact eigenvalues efficiently, but its deep, coherent circuits remain impractical for current noisy intermediate-scale quantum (NISQ) devices.[25] VQE, in contrast, employs shallow parametrized circuits with classical optimization and has been successfully demonstrated on small molecular systems.[26−30]

Within VQE, the unitary coupled cluster (UCC) ansatz,[31] derived from the coupled cluster formalism,[32] provides a physically grounded and systematically extensible representation of correlated wave functions. While classical simulations of UCC scale exponentially, its quantum implementation requires

Received: November 14, 2025
Revised: January 11, 2026
Accepted: January 12, 2026
Published: February 10, 2026

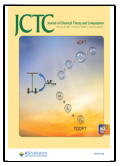

ACS Publications © 2026 American Chemical Society

https://doi.org/10.1021/acs.jctc.5c01911
J. Chem. Theory Comput. 2026, 22, 1760−1769

only polynomial resources, making it a natural foundation for chemically realistic quantum algorithms.

Recent work has unified NEO theory with quantum algorithms via multicomponent UCC (mcUCC) ansätze, enabling beyond-BO simulations that explicitly include quantum nuclear motion in both the reference and variational spaces.[33−38] This NEO−quantum computing (NEO-QC) framework provides a rigorous route to first-principles modeling of electronic−nuclear correlated systems, including positronic and protonic species, where classical approximations fail.

However, the accuracy of hybrid quantum−classical algorithms on present-day devices remains constrained by noise and decoherence. Full quantum error correction is not yet feasible, but quantum error mitigation (QEM) methods can substantially reduce systematic bias without fault-tolerant overhead. Among the most widely used are zero-noise extrapolation (ZNE), which estimates noise-free observables by deliberate noise amplification and extrapolation,[39,40] and probabilistic error cancellation (PEC), which reconstructs unbiased estimators via quasi-probability sampling.[40] Complementary strategies such as symmetry verification[41] and virtual (state) distillation[42] have further improved accuracy in quantum chemistry experiments on real hardware.[43−45]

In this work, we employ our recently developed, physically motivated error mitigation approach, Physics-Inspired Extrapolation (PIE), which extends the ZNE framework by deriving its functional form from restricted quantum dynamics.[46,47] PIE provides an interpretable extrapolation model, mitigates overfitting, and reduces sampling overhead relative to polynomial ZNE, enabling chemically accurate energy estimates for beyond-BO benchmarks on current NISQ hardware.

The remainder of this paper is organized as follows. Section 2 introduces the NEO Hamiltonian and working equations. Section 3 describes the mcUCC ansatz used in classical VQE simulations, which serve as surrogates for near-term quantum implementations limited by circuit depth and hardware noise. Section 4 outlines the VQE framework and Hamiltonian constructions for the positronium hydride (PsH) and molecular hydrogen with one quantum mechanical proton (HHq) systems. Section 5 presents PIE-based, error-mitigated VQE results using the Local Unitaty Cluster Jastrow (LUCJ) ansatz on IBM Q's Heron device. Finally, Section 6 summarizes the results and discusses prospects for scalable, multicomponent quantum simulations beyond the BO approximation.

2. NUCLEAR ELECTRONIC ORBITAL (NEO) FRAMEWORK

Building upon prior work establishing the foundations of mcUCC methods for quantum computation,[33] we perform simulations of the same systems on a quantum simulator and analyze the computational requirements for execution on real NISQ devices. Two model systems are considered: molecular hydrogen with one quantum mechanical proton (HHq) and positronium hydride (PsH).

In the NEO formalism, both electrons and selected light nuclei (e.g., protons or positrons) are treated quantum mechanically, while heavier nuclei remain classical. The total NEO Hartree−Fock (NEO-HF) wave function is expressed as a product of electronic and nuclear components

$$|\Psi_{\text{NEO-HF}}(\chi_e, \chi_p)\rangle = |\Phi_e(\chi_e)\rangle \otimes |\Phi_p(\chi_p)\rangle \tag{1}$$

where $\Phi_e(\chi_e)$ and $\Phi_p(\chi_p)$ are the electronic and quantum-nuclear wave functions, each expanded in their respective molecular orbital bases, χ_e and χ_p.

The total Hamiltonian for a system containing electrons, quantum nuclei, and classical nuclei is written as

$$\hat{H}_{\text{NEO}} = \hat{T}_e + \hat{T}_p + \hat{V}_{eN} + \hat{V}_{pN} + \hat{V}_{ee} + \hat{V}_{pp} + \hat{V}_{ep} + V_{NN} \tag{2}$$

where $\hat{T}_e$ and $\hat{T}_p$ are the kinetic energy operators for electrons and quantum nuclei, respectively, and the $\hat{V}$ terms represent the corresponding Coulomb interactions.

The one-particle operators are defined as

$$\hat{T}_e + \hat{V}_{eN} = \sum_{i=1}^{N_e}\left(-\frac{1}{2m_e}\nabla_i^2 - \sum_{a=1}^{N_{\text{nuc}}}\frac{Z_a}{|\mathbf{R}_a - \mathbf{r}_i^e|}\right) \tag{3}$$

$$\hat{T}_p + \hat{V}_{pN} = \sum_{I=1}^{N_p}\left(-\frac{1}{2m_p}\nabla_I^2 + \sum_{a=1}^{N_{\text{nuc}}}\frac{Z_a}{|\mathbf{R}_a - \mathbf{r}_I^p|}\right) \tag{4}$$

while the two-particle Coulomb interactions take the form

$$\hat{V}_{ee} = \sum_{i<j}^{N_e}\frac{1}{|\mathbf{r}_i^e - \mathbf{r}_j^e|} \tag{5}$$

$$\hat{V}_{pp} = \sum_{I<J}^{N_p}\frac{1}{|\mathbf{r}_I^p - \mathbf{r}_J^p|} \tag{6}$$

$$\hat{V}_{ep} = -\sum_{i=1}^{N_e}\sum_{I=1}^{N_p}\frac{1}{|\mathbf{r}_i^e - \mathbf{r}_I^p|} \tag{7}$$

Here, indices i, j denote electrons, I, J denote quantum nuclei, and $\mathbf{r}$ represents particle coordinates. Z_a and $\mathbf{R}_a$ denote the charge and position of the ath classical nucleus, ∇ is the Laplacian operator, and m_e and m_p are the electron and quantum-nuclear masses, respectively. The classical nucleus−nucleus repulsion is given by

$$V_{NN} = \sum_{a<b}^{N_{\text{nuc}}}\frac{Z_a Z_b}{|\mathbf{R}_a - \mathbf{R}_b|} \tag{8}$$

which is constant for a fixed nuclear geometry.

For practical computations, these operators are expressed in a finite one-particle basis $\{\phi\}$ in terms of one- and two-particle integrals. The one-particle matrix elements are

$$h_{ij} = \int \phi_i^*(\mathbf{r}^e)\left(-\frac{1}{2m_e}\nabla^2 - \sum_{a=1}^{N_{\text{nuc}}}\frac{Z_a}{|\mathbf{R}_a - \mathbf{r}^e|}\right)\phi_j(\mathbf{r}^e)\mathrm{d}\mathbf{r}^e \tag{9}$$

$$h_{IJ} = \int \phi_I^*(\mathbf{r}^p)\left(-\frac{1}{2m_p}\nabla^2 + \sum_{a=1}^{N_{\text{nuc}}}\frac{Z_a}{|\mathbf{R}_a - \mathbf{r}^p|}\right)\phi_J(\mathbf{r}^p)\mathrm{d}\mathbf{r}^p \tag{10}$$

and the two-particle integrals are

$$h_{ijkl} = \int \phi_i^*(\mathbf{r}_1^e)\phi_j^*(\mathbf{r}_2^e)\frac{1}{|\mathbf{r}_1^e - \mathbf{r}_2^e|}\phi_k(\mathbf{r}_1^e)\phi_l(\mathbf{r}_2^e)\mathrm{d}\mathbf{r}_1^e\mathrm{d}\mathbf{r}_2^e \tag{11}$$

https://doi.org/10.1021/acs.jctc.5c01911
J. Chem. Theory Comput. 2026, 22, 1760−1769

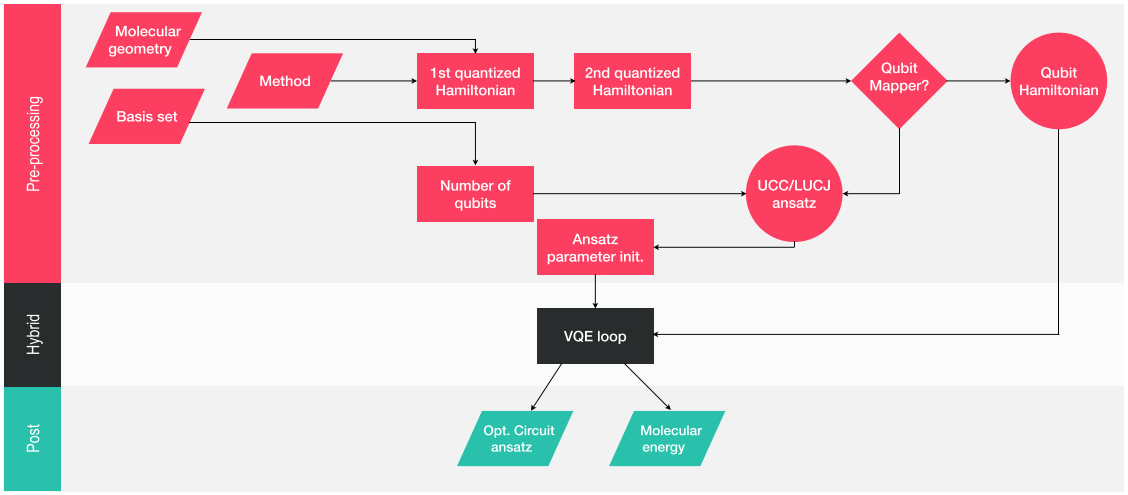

Figure 1. Schematic representation of the (VQE) algorithm. The molecular Hamiltonian is precomputed classically, while the quantum device evaluates expectation values and supplies energy feedback to the classical optimizer.

$$h_{IJKL} = \int \phi_I^*(\mathbf{r}_1^p)\phi_J^*(\mathbf{r}_2^p)\frac{1}{|\mathbf{r}_1^p - \mathbf{r}_2^p|}\phi_K(\mathbf{r}_1^p)\phi_L(\mathbf{r}_2^p)\mathrm{d}\mathbf{r}_1^p\mathrm{d}\mathbf{r}_2^p \tag{12}$$

$$h_{iIkJ} = \int \phi_i^*(\mathbf{r}^e)\phi_I^*(\mathbf{r}^p)\frac{1}{|\mathbf{r}^e - \mathbf{r}^p|}\phi_k(\mathbf{r}^e)\phi_J(\mathbf{r}^p)\mathrm{d}\mathbf{r}^e\mathrm{d}\mathbf{r}^p \tag{13}$$

This multicomponent Hamiltonian mirrors the structure of the conventional electronic Hamiltonian, with distinct one- and two-particle contributions, while extending it to include explicit electronic−nuclear and nuclear−nuclear interaction terms. Each operator term can be evaluated using standard electronic structure integrals and serves as a foundation for correlated methods that improve upon the mean-field NEO-HF energy bound.

3. COUPLED CLUSTER FORMALISM

Electronic−nuclear correlation beyond the NEO-HF level can be systematically included using the coupled cluster (CC) approach, which provides a size-extensive and systematically improvable description of correlated wave functions. The NEO-HF wave function serves as the reference state for constructing correlated multicomponent wave functions.

Gate-based quantum computers naturally implement unitary operations, making the UCC ansatz an especially suitable form of the CC method for quantum algorithms. The NEO-UCC wave function is generated by applying a unitary exponential operator[48] to the NEO-HF reference

$$|\Psi_{\text{NEO-UCC}}\rangle = e^{\hat{T}-\hat{T}^\dagger}|\Psi_{\text{NEO-HF}}\rangle \tag{14}$$

where $\hat{T}$ is the excitation operator, composed of fermionic creation ($a^\dagger$) and annihilation (a) operators weighted by variational amplitudes t. That is

$$\hat{T} = \hat{T}_1 + \hat{T}_2 + \hat{T}_3 + \cdots \tag{15}$$

where the subscript on each T denotes the order of the excitation operator. For example: $T_1 = \sum_{ia} t_i^a a_a^\dagger a_i + \sum_{IA} t_I^A a_A^\dagger a_I$, $T_2 = 1/4\sum_{ijab} t_{ij}^{ab} a_a^\dagger a_b^\dagger a_j a_i + 1/4 \sum_{IJAB} t_{IJ}^{AB} a_A^\dagger a_B^\dagger a_J a_I + \sum_{iI}^{aA} t_{iI}^{aA} a_a^\dagger a_A^\dagger a_I a_i$ and so on. Here, indices i, j, ... refer to occupied electronic orbitals, and a, b, ... to virtual electronic orbitals. For protons and positrons, uppercase indices I, J, ... and A, B, ... denote occupied and virtual protonic/positronic orbitals, respectively.

In practice, the cluster operator in eq 15 is truncated to singles and doubles (UCCSD) due to the exponential scaling of higher-order excitations. The corresponding NEO-UCC energy is obtained by minimizing the expectation value of the NEO Hamiltonian[33,49] with respect to all variational amplitudes

$$E_{\text{NEO-UCC}} = \min_{\{t\}}\langle\Psi_{\text{NEO-UCC}}|\hat{H}_{\text{NEO}}|\Psi_{\text{NEO-UCC}}\rangle \tag{16}$$

This variational formulation allows straightforward integration into hybrid quantum−classical algorithms such as the VQE, where the amplitudes $\{t\}$ are optimized iteratively using energy feedback from a quantum device.

4. VARIATIONAL QUANTUM EIGENSOLVER METHOD

4.1. Variational Quantum Eigensolver in the NEO Framework

The inclusion of electronic−nuclear correlation effects within a quantum computing framework can be achieved using the hybrid quantum−classical VQE algorithm,[26,27,29,30] schematically illustrated in Figure 1. In this approach, the molecular Hamiltonian is precomputed classically and encoded in a qubit representation, while a quantum processor evaluates expectation values for a parametrized trial wave function. The variational parameters are iteratively optimized by a classical optimizer to minimize the total energy until self-consistency is achieved.

In this work, the NEO-HF problem is first solved classically to obtain the reference orbitals and molecular integrals for a given molecular geometry and basis set. Each operator term in the NEO Hamiltonian (eq 2) is evaluated in the atomic orbital basis and subsequently transformed into the molecular orbital basis through a standard congruence transformation. The resulting Hamiltonian is then expressed in its second-quantized form.

The second-quantized Hamiltonian is mapped to qubit operators using a fermion-to-qubit transformation. Common mappings include the Jordan−Wigner[50,51] and Bravyi−Kitaev[52] transformations. In this work, both mappings were implemented using the `OpenFermion` library[53] (`openfermion.transforms.jordan_wigner` and `openfermion.transforms.bravyi_kitaev`),

https://doi.org/10.1021/acs.jctc.5c01911
J. Chem. Theory Comput. 2026, 22, 1760−1769

with results reported primarily using the Jordan–Wigner transformation.

Parallel to the Hamiltonian encoding, the multicomponent CC excitation operators (singles, doubles, and selected triples) are constructed classically following the mcUCC formalism.[33] These operators define the parametrized trial state used in VQE, typically in the form of a UCC ansatz with variational amplitudes serving as tunable parameters.

During VQE execution, the quantum circuit corresponding to the chosen ansatz is evaluated on a quantum backend or simulator, such as those provided in `Qiskit`.[54] The expectation value of the energy is computed as

$$E(\boldsymbol{\theta}) = \langle \Psi(\boldsymbol{\theta}) | \hat{H}_{\mathrm{NEO}} | \Psi(\boldsymbol{\theta}) \rangle \tag{17}$$

where $\boldsymbol{\theta}$ represents the set of variational parameters. A classical optimizer (e.g., COBYLA or SPSA) updates $\boldsymbol{\theta}$ iteratively to minimize the energy

$$E_{\min} = \min_{\boldsymbol{\theta}} E(\boldsymbol{\theta}) \tag{18}$$

This iterative feedback loop continues until the convergence criterion is met, yielding the lowest energy consistent with the chosen ansatz and hardware precision.

4.2. Implementation for Representative Systems

A minimal basis is employed for each system to capture the essential physics while keeping computational cost manageable (Figure 2). For the HHq system, this corresponds to an STO-3G basis (two s-type orbitals)[55] for the electrons and a 2s basis with exponents 4 and 8 for the proton.[33] In the case of PsH, a 6–31G basis (two s-type orbitals)[56] is used for both the electrons and the positron. Although this work focuses on these minimal systems, the same workflow is readily extendable to larger basis sets and other multicomponent molecular systems.

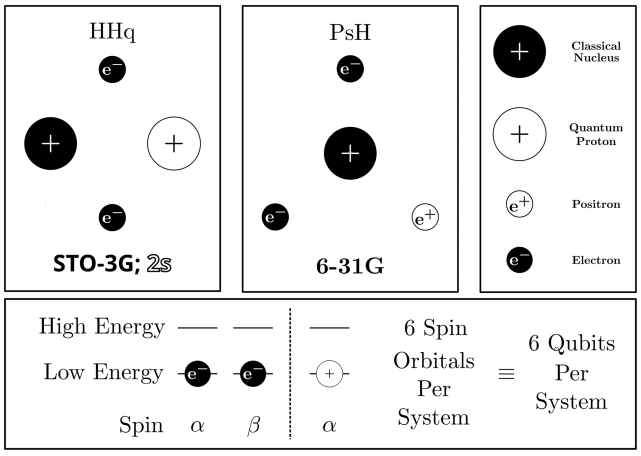

Figure 2. Top: Schematic representations of the hydrogen molecule with a quantum mechanical proton (HHq) and positronium hydride (PsH). Bottom: Spin orbital configurations for both systems under the chosen bases: 6-31G for electronic and positronic orbitals in PsH; STO-3G for electronic orbitals and 2s for protonic orbital in HHq.

Each system comprises six spin orbitals and three quantum particles: (i) PsH, containing two quantum electrons and one quantum positron; and (ii) HHq, containing two quantum electrons and one quantum nucleus. Each electron contributes two spin orbitals, while the positron or quantum proton contributes two spatial orbitals. The orbital arrangement and particle composition are depicted in Figure 2.

To reduce circuit depth and gate count for near-term quantum implementation, we consider two strategies. First, only spin-conserving excitations are included for the electronic subspace, while the positron and quantum proton are both fixed to the α spin state. In a minimal basis, the second-quantized CC excitation operators restricted to spin-allowed transitions are given by

$$t_{1e} = (t_0^2 c_2^\dagger c_0 - t_2^0 c_0^\dagger c_2) + (t_1^3 c_3^\dagger c_1 - t_3^1 c_1^\dagger c_3) \tag{19}$$

$$t_{1p} = (t_4^5 c_5^\dagger c_4 - t_5^4 c_4^\dagger c_5) \tag{20}$$

$$t_{2ee} = (t_{01}^{23} c_2^\dagger c_3^\dagger c_1 c_0 - t_{23}^{01} c_0^\dagger c_1^\dagger c_3 c_2) \tag{21}$$

$$t_{2ep} = (t_{04}^{25} c_2^\dagger c_5^\dagger c_4 c_0 - t_{25}^{04} c_0^\dagger c_4^\dagger c_5 c_2) + (t_{14}^{35} c_3^\dagger c_5^\dagger c_4 c_1 - t_{35}^{14} c_1^\dagger c_4^\dagger c_5 c_3) \tag{22}$$

$$t_{3eep} = (t_{014}^{235} c_2^\dagger c_3^\dagger c_5^\dagger c_4 c_1 c_0 - t_{235}^{014} c_0^\dagger c_1^\dagger c_4^\dagger c_5 c_3 c_2) \tag{23}$$

Here, indices 0–3 label electronic spin orbitals, while 4 and 5 correspond to the protonic (or positronic) spatial orbitals.

Second, calculations based on the standard unitary coupled-cluster (UCC) formalism use a selected subset of operators. Our approach is inspired by the ADAPT-VQE protocol,[57] which dynamically constructs the ansatz by selecting the most relevant UCC operators at each optimization step in order to reduce computational cost. In contrast to a fully automated ADAPT-VQE implementation, however, we manually select the operator pools considered. These pools are then used to generate the results summarized in Table 1, including the corresponding energies as well as the resulting circuit compositions and depths for representative subsets of UCC excitation operators.

5. RESULTS AND DISCUSSION

5.1. Classical Simulations

Classical simulations were performed to evaluate different combinations of cluster excitation operators, categorized by particle type (electronic or protonic/positronic) and excitation order (singles, doubles, triples). The simulations were executed on the `FakeNairobiV2` backend, a seven-qubit architecture containing one additional qubit beyond the minimum required for these systems. This device was used to assess circuit composition and resource requirements prior to deployment on real quantum hardware. Table 1 summarizes the gate counts, circuit depths, and corresponding noiseless VQE energies for each operator pool. The benchmark energy was obtained from a NEO full configuration interaction (NEO-FCI) calculation.

It is evident that the highest accuracy is obtained when all excitation operators are included; however, the resulting circuit depth and gate count far exceed the practical limits of current NISQ devices. Reducing the operator pool by truncating higher-order or mixed excitations decreases computational cost but also limits the recoverable correlation energy. When only single electronic and protonic excitations $\{t_{1e}, t_{1p}\}$ are included, the computed energy is identical to the Hartree–Fock reference, confirming that individual single excitations do not contribute to correlation energy in these systems.

https://doi.org/10.1021/acs.jctc.5c01911
J. Chem. Theory Comput. 2026, 22, 1760–1769

Table 1. Energies, Circuit Depths, and Gate Counts for the Noiseless VQE Simulations of HHq and PsH Systems Using the Jordan−Wigner Qubit Mapping, LUCJ Experiments and Classical Computer Calculations

HHq operator pool	RZ	SX	CNOT	X	total	depth	energy (Hartree)
$t_{1e}t_{1p}$	55	48	47	1	151	112	−1.059569
$t_{1p}t_{2ee}$	109	86	68	2	265	178	−1.079396
$t_{1e}t_{2ee}$	144	113	80	3	340	225	−1.079406
$t_{2ee}t_{2ep}$	211	170	115	4	500	329	−1.079421
$t_{1e}t_{1p}t_{2ee}t_{2ep}$	246	192	129	6	573	379	−1.079431
$t_{1e}t_{1p}t_{2ee}t_{2ep}t_{3eep}$	499	380	227	12	1118	743	−1.079433
LUCJ ansatz (numerical)	39	20	16	8	83	25	−1.079406
LUCJ ansatz (experimental)							−1.077 ± 0.009
NEO-HF (classical)							−1.059569
NEO-FCI (classical)							−1.079434
PsH operator pool	RZ	SX	CNOT	X	total	depth	energy (Hartree)
$t_{1e}t_{1p}$	55	48	47	1	151	112	−0.558727
$t_{1p}t_{2ee}$	107	86	68	2	263	175	−0.569124
$t_{1e}t_{2ee}$	144	113	80	3	340	224	−0.569124
$t_{2ee}t_{2ep}$	202	166	115	5	488	328	−0.572710
$t_{1e}t_{1p}t_{2ee}t_{2ep}$	234	188	129	7	558	373	−0.572710
$t_{1e}t_{1p}t_{2ee}t_{2ep}t_{3eep}$	475	366	227	14	1082	727	−0.572714
LUCJ ansatz (numerical)	55	34	20	3	112	43	−0.569178
LUCJ ansatz (experimental)							−0.55 ± 0.03
NEO-HF (classical)							−0.558727
NEO-FCI (classical)							−0.572838

Intermediate levels of correlation can be recovered by including double excitations. For HHq, using $\{t_{1e}, t_{2ee}\}$ yields an energy of −1.079406 Ha, sufficient for chemical accuracy and closely matching the NEO-FCI limit. Adding mixed electron−proton double excitations $\{t_{2ee}, t_{2ep}\}$ further lowers the energy by approximately 15 μHa, reducing the deviation from the FCI value to about 13 μHa. This agrees with previous results for H_2 in a minimal STO-3G basis, where inclusion of the double electronic excitation operator alone recovers nearly the full correlation energy.[57]

For HHq, the electron−proton correlation contribution is significantly smaller than the electron−electron correlation term (10^{-5} vs 10^{-2} Ha), due to the large proton mass. In contrast, in PsH the electronic−positronic correlation energy is comparable to the electron−electron correlation energy (i.e., $E_{\{t_{2ee}t_{2ep}\}} = -0.572710$ Ha relative to $E_{\{t_{1e}t_{2ee}\}} = -0.569124$ Ha is similar to the latter relative to $E_{\{t_{1e}t_{1p}\}} = -0.558727$ Ha). This arises from the comparable masses of the electron and positron, which yield matrix elements of similar magnitude. In HHq, the corresponding mixed terms are suppressed by the proton−electron mass ratio (∼2000), reducing the overall protonic correlation contribution. These trends suggest that a balanced trade-off between computational cost and accuracy can be achieved by including electronic and mixed electron−positron double excitations, which effectively capture correlation while maintaining feasible circuit depth.

To relate circuit complexity to hardware constraints, we adopt the heuristic introduced by Leymann and Barzen[58]

$$d \cdot w \ll \frac{1}{\epsilon} \tag{24}$$

where d and w denote circuit depth and width, respectively, and ϵ is the average gate error rate. This inequality expresses the qualitative requirement for executing a quantum circuit before decoherence dominates. While this metric does not prescribe an accuracy target, the statistical precision of energy measurements can be improved by increasing the number of measurement shots.

As an illustrative estimate, approximately 170 gates would be required to achieve a target precision of 0.001 Ha for a six-qubit circuit. However, in practice, even single-excitation UCC ansätze already entail ∼47 CNOT gates, exceeding the realistic depth limits of current NISQ hardware. Consequently, accurate beyond-BO quantum simulations remain computationally prohibitive on existing devices. Detailed resource requirements and corresponding energy estimates are provided in Table 1.

5.2. Demonstration on IBM Q

To demonstrate the feasibility of multicomponent quantum simulations on real hardware, we employed the Local Unitary Cluster Jastrow (LUCJ) ansatz,[59] a variational wave function specifically designed for correlated electronic ground states on near-term quantum processors. The LUCJ ansatz captures both dynamic and static correlation effects while substantially reducing circuit depth and two-qubit gate requirements compared to traditional quantum chemistry ansätze such as quadratic unitary coupled cluster singles and doubles (qUCCSD).

Unlike qUCCSD, which involves deep, nonlocal circuits with many variational parameters, the LUCJ ansatz starts from a restricted Hartree−Fock reference and applies a physically motivated correlator inspired by the repulsive Hubbard model. By penalizing double occupancy on the same spatial orbital (opposite-spin electrons) and restricting correlations to local

https://doi.org/10.1021/acs.jctc.5c01911
J. Chem. Theory Comput. 2026, 22, 1760−1769

orbital neighborhoods, the LUCJ formulation balances accuracy and hardware efficiency.

The general LUCJ wave function is constructed as a product of L local layers

$$|\Psi\rangle = \prod_{\mu=1}^{L} e^{\hat{K}_\mu} e^{i\hat{J}_\mu} e^{-\hat{K}_\mu} |\Psi_{\text{NEO-HF}}\rangle \tag{25}$$

where

$$\hat{K}_\mu = \sum_{s,\sigma} K_s^\mu \hat{a}_{s\sigma}^\dagger \hat{a}_{s\sigma}, \quad \hat{J}_\mu = \sum_{s,\sigma\tau} J_{s,\sigma\tau}^\mu \hat{n}_{s\sigma} \hat{n}_{s\tau} \tag{26}$$

Here, $\hat{K}_\mu$ and $\hat{J}_\mu$ represent one-body rotation and two-body number−number correlation operators, respectively, with s indexing spatial orbitals and σ, τ denoting spin. For simplicity, all quantum particles (electrons, positrons, and quantum nuclei) are represented by a unified orbital index s. This convention is followed in Figures 3, 4, and 6.

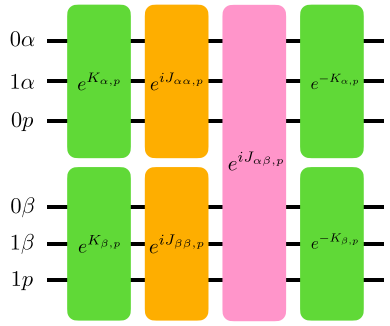

Figure 3. Example circuit block for the LUCJ ansatz applied to PsH, following eq 25. Orbitals {0, 1} correspond to the two electronic spatial orbitals, while p labels the positron without any spin orbital. The complete circuit decomposition is shown in Figures 4 and 6.

Because the circuit depth required by UCC-based approaches remains prohibitive for current hardware, we employ a single LUCJ layer ($L = 1$) to approximate the ground-state energies of HHq and PsH. This ansatz achieves a ∼57% reduction in CNOT gate count relative to the minimal UCC ansatz including $\{t_{1\alpha}, t_{1p}\}$ excitations, while maintaining comparable accuracy (see Table 1).

The LUCJ circuits were implemented and executed on the 133-qubit IBM Q Heron superconducting processor (ibm torino). A six-qubit subset was selected, as shown in Figures 4 and 6, to represent the low- and high-energy electron spin orbitals (0α, 0β, 1α, 1β) and the positron/nucleus spatial orbitals (0p and 1p). Only local two-qubit operations between adjacent qubits were used, respecting the device topology and minimizing cross-talk.

5.3. Quantum Error Mitigation via Physics-Inspired Extrapolation (PIE)

To mitigate hardware noise, we implemented our recently proposed Physics-Inspired Extrapolation (PIE) method[47] (see the Appendix A and Algorithm 1). PIE builds on the Error Mitigation by Restricted Evolution (EMRE) framework,[46] which provides an analytical form for the extrapolation function used to recover noise-free observables. Unlike polynomial extrapolation, PIE yields interpretable extrapolation parameters, constant runtime scaling, and reduced sampling overhead. In PIE, noise is systematically amplified via circuit folding, and expectation values are measured at multiple noise levels. The results are then extrapolated to the zero-noise limit using a linearized model derived from EMRE. Depending on circuit complexity, full or partial folding is employed to achieve controlled noise amplification.

The experimental execution of the LUCJ circuits and the implementation of the error mitigation protocol are shown in Figure 5. Optimal LUCJ parameters were first obtained through noiseless classical simulations, yielding energies of −1.079406 Ha for HHq and −0.569178 Ha for PsH. The corresponding quantum circuits were then executed on the ibm torino processor using 4096 shots per circuit. Noisy runs produced raw energies of −0.996468 ± 0.013563 Ha (HHq) and −0.393893 ± 0.013127 Ha (PsH), indicated by the experimental data at $\lambda = 1$ in Figure 5. After applying PIE-based error mitigation, the extrapolated energies improved to −1.076668 ± 0.009229 Ha and −0.551371 ± 0.031024 Ha, respectively. These mitigated results are denoted by red dots at $\lambda = 0$ in Figure 5. Uncertainties correspond to the standard deviation from repeated runs. The experimental result is significantly lower than the NEO-HF energy for HHq, but it is similar to the NEO-HF energy for PsH, although the uncertainties encompass the NEO-FCI energy.

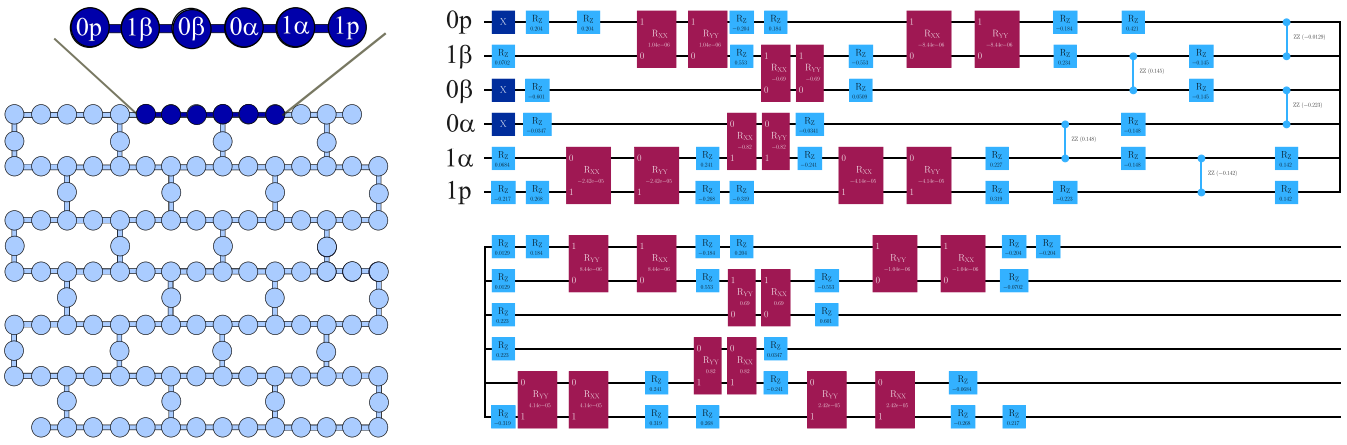

Figure 4. (Left) Topology of the 133-qubit IBM Heron superconducting processor (ibm torino); the 6-qubit subset used for the demonstration is highlighted in dark blue. (Right) LUCJ circuit expressed in the {*rz*, *rxx*, *ryy*, *rzz*, *x*} gate basis. Each qubit corresponds to one spatial or spin orbital, and the circuit is initialized in the NEO-HF reference state. See Figure 6 for legible drawing of the circuit.

https://doi.org/10.1021/acs.jctc.5c01911
J. Chem. Theory Comput. 2026, 22, 1760−1769

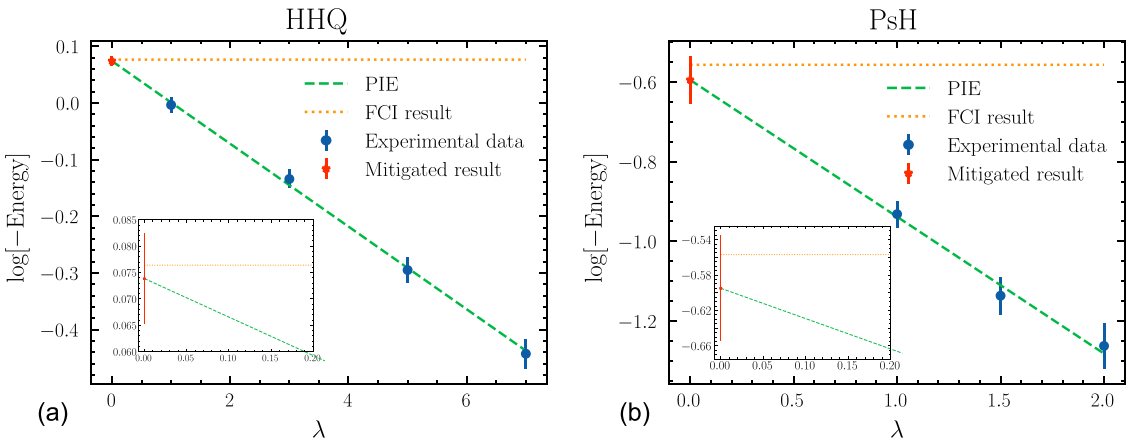

Figure 5. Extrapolated energy results using the PIE method for (a) HHq and (b) PsH. The logarithm of the negative energy is plotted as a function of the number of circuit foldings, with the zero-noise limit obtained from a linear fit. Raw quantum circuit executions correspond to experimental data at $\lambda = 1$, while the noise-mitigated energies are denoted by red dots at $\lambda = 0$.

The error-mitigated results achieved with the LUCJ ansatz and PIE are chemically accurate, closely matching the classical VQE results obtained using the $\{t_{1e}, t_{2ee}\}$ UCC operator set, while requiring substantially fewer gates. Although the results remain several millihartrees above the FCI limit for HHq and around 20 millihartrees above the FCI limit for PsH, this demonstration highlights the viability of combining physically motivated ansätze and advanced error mitigation to achieve multicomponent quantum simulations on current NISQ hardware.

6. CONCLUDING REMARKS

In this work, we carried out multicomponent electronic structure calculations for positronium hydride (PsH) and dihydrogen with a quantum mechanical proton (HHq) using quantum computing frameworks. Simulations on a quantum computer emulator enabled us to systematically assess the contributions of different excitation operators within the mcUCC ansatz and to quantify the correlation energy recovered under various truncation schemes.

In addition, we performed experimental demonstrations on IBM's superconducting quantum hardware using the Local Unitary Cluster Jastrow ansatz in combination with the Physics-Inspired Extrapolation error mitigation technique. This hybrid strategy achieved chemically accurate ground-state energies for both PsH and HHq while operating within the resource constraints of current noisy intermediate-scale quantum devices. The LUCJ ansatz provided a compact, hardware-efficient alternative to traditional coupled-cluster-based ansätze, and PIE successfully mitigated hardware noise to recover high-fidelity energies from noisy measurements.

Together, these results demonstrate a viable path toward scalable, beyond-Born−Oppenheimer quantum simulations that explicitly incorporate nuclear quantum effects. By combining physically motivated ansätze, resource-efficient circuit constructions, and advanced error mitigation, this work establishes a foundation for accurate, multicomponent quantum chemistry on near-term quantum processors and offers a roadmap toward chemically relevant quantum simulations in the NISQ era.

APPENDIX

A. Physics-Inspired Extrapolation (PIE)

PIE looks operationally like zero-noise extrapolation (ZNE) (i.e., collect data under noise amplification), but uses a model derived from error mitigation by restricted evolution (EMRE) plus an information-theoretic quantity (the max-relative entropy). The practical consequence is that the extrapolation becomes *log−linear*, which tends to be stable, and the slope has a physical interpretability.

Workflow

1. Choose a target circuit and an observable O.
2. Create *noise-amplified* versions of the circuit using folding (insert identity-equivalent blocks so the ideal unitary is unchanged, while noise accumulates).
3. Measure $\langle O \rangle$ at several fold levels.
4. Fit $\log(\langle O \rangle)$ versus fold count to a straight line.
5. Extrapolate to "zero folds" using the fitted intercept to estimate the noise-free expectation value. Interpret the slope as a hardware/noise diagnostic.

A.1. Noise Amplification via Circuit Folding

The paper uses **global circuit folding**. The core idea is to keep the ideal unitary U fixed while increasing the number of noisy operations executed. One common folding pattern is

$$U \rightarrow U(U^{\dagger}U)^{n} \tag{27}$$

which is exactly U in the absence of noise, but increases physical noise accumulation when implemented on real hardware.

This produces data points

$$\langle O \rangle(n),\ n = 0, 1, 2, \ldots$$

that can be used for extrapolation.

A.2. Folding and the Emergence of a Log−Linear Relationship

Folding effectively repeats the noisy process. Under assumptions that the relevant distance parameter accumulates predictably with the number of folds, one obtains a relationship of the schematic form

$$\langle O \rangle(n) \approx \langle O \rangle_{\text{ideal}}\, e^{-\alpha n} \tag{28}$$

https://doi.org/10.1021/acs.jctc.5c01911
J. Chem. Theory Comput. 2026, 22, 1760−1769

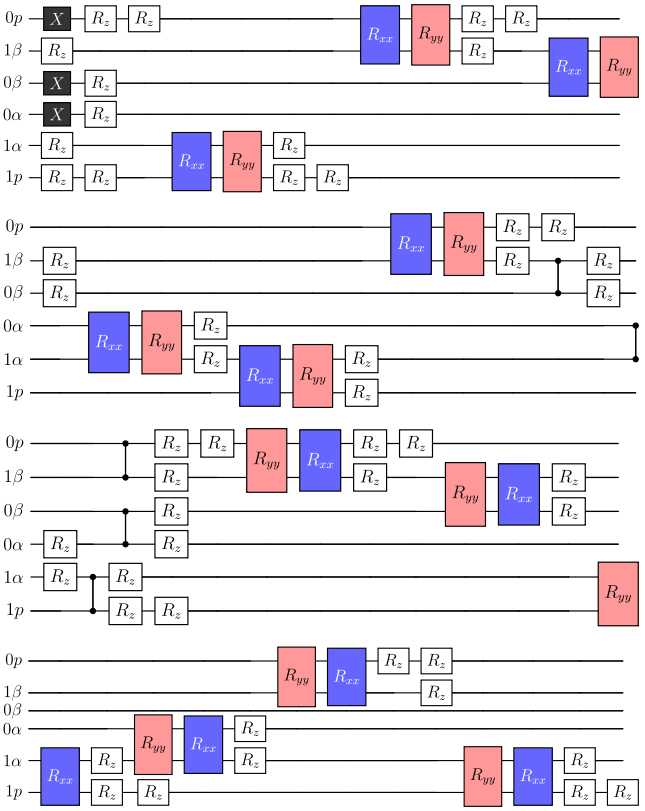

Figure 6. Ansatz circuit used in our IBM Q experiments.

where the decay rate α is tied to the max-relative entropy (up to conventions, log base, and approximations).

Taking the logarithm yields a **linear model in** n

$$\log|\langle O\rangle(n)| \approx \underbrace{\log|\langle O\rangle_{\text{ideal}}|}_{\text{intercept}} - \underbrace{\alpha}_{\text{slope}}\, n \tag{29}$$

Interpretation:

- The intercept estimates the (log) noise-free expectation value.
- The slope estimates an effective "distance"/noise-strength parameter related to $D_{\max}$, offering a hardware-diagnostic ("certification") angle.

Sign handling: if $\langle O\rangle(n)$ can become negative, one can fit $\log|\langle O\rangle(n)|$ and restore the sign using, e.g., the sign of the $n = 0$ value or a separate sign-tracking rule.

A.3. Conceptual Takeaway

PIE can be summarized as *Collect ZNE-style folded-circuit data, but fit a model whose form is motivated by EMRE which inherently has the channel max-relative entropy built into it, yielding a robust log−linear extrapolation where the slope has a physical meaning.*

The emphasis is dual-purpose:

- **Error mitigation:** improved stability and accuracy compared to heuristic extrapolation choices.
- **Certification/diagnostics:** interpret the fitted slope as a measure of noise strength related to a channel distance (max-relative entropy).

Algorithm 1 PIE minimal implementation recipe

Require: Quantum circuit $\mathcal{C}$, observable O, shot budget S, fold set $\mathcal{N}$ (e.g. $\{0,1,2,3\}$)
Ensure: Mitigated estimate $\widehat{\langle O\rangle}_{\text{ideal}}$ and slope parameter $\widehat{\alpha}$
Choose fold counts $\mathcal{N} \leftarrow \{0,1,2,3\}$ {or any small set of nonnegative integers}
for all $n \in \mathcal{N}$ **do**
  Construct globally folded circuit $\mathcal{C}^{(n)} \leftarrow \text{Fold}(\mathcal{C}, n)$
  Execute $\mathcal{C}^{(n)}$ for S shots and estimate $\langle O\rangle(n)$
  Compute $y_n \leftarrow \log|\langle O\rangle(n)|$
end for
Fit $\{(n, y_n)\}_{n\in\mathcal{N}}$ to the linear model $y_n = a + bn$ (least squares or robust regression)
Set $\widehat{\langle O\rangle}_{\text{ideal}} \leftarrow \text{sign}(\langle O\rangle(0))\, e^{a}$
Set $\widehat{\alpha} \leftarrow -b$ {effective slope parameter (noise-related)}
return $\left(\widehat{\langle O\rangle}_{\text{ideal}}, \widehat{\alpha}\right)$

AUTHOR INFORMATION

Corresponding Authors

Thi Ha Kyaw − *LG Electronics Toronto AI Lab, Toronto, Ontario M5V 1M3, Canada;* orcid.org/0000-0002-3557-2709; Email: thiha.kyaw@lge.com

Victor S. Batista − *Department of Chemistry, Yale University, New Haven, Connecticut 06520, United States; Yale Quantum Institute, Yale University, New Haven, Connecticut 06511, United States;* orcid.org/0000-0002-3262-1237; Email: victor.batista@yale.edu

Authors

Delmar G. A Cabral − *Department of Chemistry, Yale University, New Haven, Connecticut 06520, United States;* orcid.org/0009-0001-1195-5529

Brandon Allen − *Department of Chemistry, Yale University, New Haven, Connecticut 06520, United States;* orcid.org/0000-0002-5512-1892

Fabijan Pavošević − *Algorithmiq Ltd., FI-00160 Helsinki, Finland;* orcid.org/0000-0002-3693-7546

Sharon Hammes-Schiffer − *Department of Chemistry, Princeton University, Princeton, New Jersey 08540, United States;* orcid.org/0000-0002-3782-6995

Pablo Díez-Valle − *Instituto Tecnológico de Galicia, 15003 A Coruña, Spain*

Jack S. Baker − *LG Electronics Toronto AI Lab, Toronto, Ontario M5V 1M3, Canada*

Gaurav Saxena − *LG Electronics Toronto AI Lab, Toronto, Ontario M5V 1M3, Canada*

Complete contact information is available at: https://pubs.acs.org/10.1021/acs.jctc.5c01911

Notes

The authors declare no competing financial interest.

ACKNOWLEDGMENTS

This material is based upon work supported by the National Science Foundation for the Center for Quantum Dynamics on Modular Quantum Devices, grant numbers CHE-2124511 and CHE-2408934 (SHS).

REFERENCES

(1) Garrett, B. C.; Truhlar, D. G. Accuracy of tunneling corrections to transition state theory for thermal rate constants of atom transfer reactions. *J. Phys. Chem. A* **1979**, *83*, 200−203.

(2) Klinman, J. P.; Kohen, A. Hydrogen Tunneling Links Protein Dynamics to Enzyme Catalysis. *Annu. Rev. Biochem.* **2013**, *82*, 471−496.

(3) Layfield, J. P.; Hammes-Schiffer, S. Hydrogen Tunneling in Enzymes and Biomimetic Models. *Chem. Rev.* **2014**, *114*, 3466−3494.

(4) Meisner, J.; Kästner, J. Atom Tunneling in Chemistry. *Angew. Chem., Int. Ed.* **2016**, *55*, 5400−5413.

(5) Hammes-Schiffer, S. Proton-Coupled Electron Transfer: Moving Together and Charging Forward. *J. Am. Chem. Soc.* **2015**, *137*, 8860−8871.
(6) Tyburski, R.; Liu, T.; Glover, S. D.; Hammarström, L. Proton-Coupled Electron Transfer Guidelines, Fair and Square. *J. Am. Chem. Soc.* **2021**, *143*, 560−576.
(7) Hammes-Schiffer, S. Exploring Proton-Coupled Electron Transfer at Multiple Scales. *Nat. Comput. Sci.* **2023**, *3*, 291−300.
(8) Waluk, J. Nuclear Quantum Effects in Proton or Hydrogen Transfer. *J. Phys. Chem. Lett.* **2024**, *15*, 598−607.
(9) Webb, S. P.; Iordanov, T.; Hammes-Schiffer, S. Multiconfigurational Nuclear-Electronic Orbital Approach: Incorporation of Nuclear Quantum Effects in Electronic Structure Calculations. *J. Chem. Phys.* **2002**, *117*, 4106−4118.
(10) Hammes-Schiffer, S. Nuclear−Electronic Orbital Methods: Foundations and Prospects. *J. Chem. Phys.* **2021**, *155*, No. 030901.
(11) Pak, M. V.; Chakraborty, A.; Hammes-Schiffer, S. Density Functional Theory Treatment of Electron Correlation in the Nuclear-Electronic Orbital Approach. *J. Phys. Chem. A* **2007**, *111*, 4522−4526.
(12) Yang, Y.; Brorsen, K. R.; Culpitt, T.; Pak, M. V.; Hammes-Schiffer, S. Development of a practical multicomponent density functional for electron-proton correlation to produce accurate proton densities. *J. Chem. Phys.* **2017**, *147*, No. 114113.
(13) Xu, X.; Yang, Y. Constrained nuclear-electronic orbital density functional theory: Energy surfaces with nuclear quantum effects. *J. Chem. Phys.* **2020**, *152*, No. 084107.
(14) Hasecke, L.; Mata, R. A. Nuclear Quantum Effects Made Accessible: Local Density Fitting in Multicomponent Methods. *J. Chem. Theory Comput.* **2023**, *19*, 8223−8233.
(15) Pavošević, F.; Culpitt, T.; Hammes-Schiffer, S. Multicomponent Coupled Cluster Singles and Doubles Theory within the Nuclear-Electronic Orbital Framework. *J. Chem. Theory Comput.* **2019**, *15*, 338−347.
(16) Brorsen, K. R. Quantifying Multireference Character in Multicomponent Systems with Heat-Bath Configuration Interaction. *J. Chem. Theory Comput.* **2020**, *16*, 2379−2388.
(17) Hasecke, L.; Mata, R. A. Local Electronic Correlation in Multicomponent Møller-Plesset Perturbation Theory. *J. Chem. Theory Comput.* **2024**, *20*, 9928−9938.
(18) Malbon, C. L.; Hammes-Schiffer, S. Nuclear-Electronic Orbital Multireference Configuration Interaction for Ground and Excited Vibronic States and Fundamental Insights into Multicomponent Basis Sets. *J. Chem. Theory Comput.* **2025**, *21*, 3968−3980.
(19) Goudy, R. J.; Pavošević, F.; Hammes-Schiffer, S. Triple excitations in nuclear-electronic orbital coupled cluster theory for multiple quantum protons. *J. Chem. Phys.* **2025**, *163*, No. 224119.
(20) Abrams, D. S.; Lloyd, S. Simulation of Many-Body Fermi Systems on a Universal Quantum Computer. *Phys. Rev. Lett.* **1997**, *79*, No. 2586.
(21) Aspuru-Guzik, A.; Dutoi, A. D.; Love, P. J.; Head-Gordon, M. Simulated Quantum Computation of Molecular Energies. *Science* **2005**, *309*, 1704−1707.
(22) Cao, Y.; Romero, J.; Olson, J. P.; Degroote, M.; Johnson, P. D.; Kieferová, M.; Kivlichan, I. D.; Menke, T.; Peropadre, B.; Sawaya, N. P. D.; Sukin, S.; Veis, L.; Aspuru-Guzik, A. Quantum Chemistry in the Age of Quantum Computing. *Chem. Rev.* **2019**, *119*, 10856−10915.
(23) Bauer, B.; Bravyi, S.; Motta, M.; Kin-Lic Chan, G. Quantum Algorithms for Quantum Chemistry and Quantum Materials Science. *Chem. Rev.* **2020**, *120*, 12685−12717.
(24) Bharti, K.; Cervera-Lierta, A.; Kyaw, T. H.; Haug, T.; Alperin-Lea, S.; Anand, A.; Degroote, M.; Heimonen, H.; Kottmann, J. S.; Menke, T.; Mok, W.-K.; Sim, S.; Kwek, L.-C.; Aspuru-Guzik, A. Noisy Intermediate-Scale Quantum Algorithms. *Rev. Mod. Phys.* **2022**, *94*, No. 015004.
(25) Preskill, J. Quantum Computing in the NISQ Era and Beyond. *Quantum* **2018**, *2*, No. 79.
(26) Peruzzo, A.; McClean, J.; Shadbolt, P.; Yung, M.-H.; Zhou, X.-Q.; Love, P. J.; Aspuru-Guzik, A.; O'brien, J. L. A Variational Eigenvalue Solver on a Photonic Quantum Processor. *Nat. Commun.* **2014**, *5*, No. 4213.
(27) O'Malley, P. J. J.; Babbush, R.; Kivlichan, I. D.; Romero, J.; McClean, J. R.; Barends, R.; Kelly, J.; Roushan, P.; Tranter, A.; Ding, N. Scalable Quantum Simulation of Molecular Energies. *Phys. Rev. X* **2016**, *6*, No. 031007.
(28) Kandala, A.; Mezzacapo, A.; Temme, K.; Takita, M.; Brink, M.; Chow, J. M.; Gambetta, J. M. Hardware-Efficient Variational Quantum Eigensolver for Small Molecules and Quantum Magnets. *Nature* **2017**, *549*, 242−246.
(29) Hempel, C.; Maier, C.; Romero, J.; McClean, J.; Monz, T.; Shen, H.; Jurcevic, P.; Lanyon, B. P.; Love, P.; Babbush, R.; et al. Quantum Chemistry Calculations on a Trapped-Ion Quantum Simulator. *Phys. Rev. X* **2018**, *8*, No. 031022.
(30) Romero, J.; Babbush, R.; McClean, J. R.; Hempel, C.; Love, P. J.; Aspuru-Guzik, A. Strategies for Quantum Computing Molecular Energies Using the Unitary Coupled Cluster Ansatz. *Quantum Sci. Technol.* **2019**, *4*, No. 014008.
(31) Anand, A.; Schleich, P.; Alperin-Lea, S.; Jensen, P. W. K.; Sim, S.; Díaz-Tinoco, M.; Kottmann, J. S.; Degroote, M.; Izmaylov, A. F.; Aspuru-Guzik, A. A Quantum Computing View on Unitary Coupled Cluster Theory. *Chem. Soc. Rev.* **2022**, *51*, 1659−1684.
(32) Coester, F.; Kümmel, H. Short-Range Correlations in Nuclear Wave Functions. *Nucl. Phys.* **1960**, *17*, 477−485.
(33) Pavošević, F.; Hammes-Schiffer, S. Multicomponent Unitary Coupled Cluster and Equation-of-Motion for Quantum Computation. *J. Chem. Theory Comput.* **2021**, *17*, 3252−3258.
(34) Kovyrshin, A.; Skogh, M.; Tornberg, L.; Broo, A.; Mensa, S.; Sahin, E.; Symons, B. C. B.; Crain, J.; Tavernelli, I. Nonadiabatic Nuclear−Electron Dynamics: A Quantum Computing Approach. *J. Phys. Chem. Lett.* **2023**, *14*, 7065−7072.
(35) Nykänen, A.; Miller, A.; Talarico, W.; Knecht, S.; Kovyrshin, A.; Skogh, M.; Tornberg, L.; Broo, A.; Mensa, S.; Symons, B. C. B.; Sahin, E.; Crain, J.; Tavernelli, I.; Pavošević, F. Toward Accurate Post-Born−Oppenheimer Molecular Simulations on Quantum Computers: An Adaptive Variational Eigensolver with Nuclear-Electronic Frozen Natural Orbitals. *J. Chem. Theory Comput.* **2023**, *19*, 9269−9277.
(36) Kovyrshin, A.; Skogh, M.; Broo, A.; Mensa, S.; Sahin, E.; Crain, J.; Tavernelli, I. A Quantum Computing Implementation of Nuclearelectronic Orbital (NEO) Theory: Toward an Exact Pre-Born−Oppenheimer Formulation of Molecular Quantum Systems. *J. Chem. Phys.* **2023**, *158*, No. 214119, DOI: 10.1063/5.0150291.
(37) Kovyrshin, A.; Manawadu, D.; Altamura, E.; Pennington, G.; Jaderberg, B.; Brandhofer, S.; Nykänen, A.; Miller, A.; Talarico, W.; Knecht, S.; Pavošević, F.; Baiardi, A.; Tacchino, F.; Tavernelli, I.; Mensa, S.; Crain, J.; Tornberg, L.; Broo, A. Approximate Quantum Circuit Compilation For Proton-Transfer Kinetics On Quantum Processors, arXiv:2507.08996. arXiv.org e-Print archive, 2025 https://arxiv.org/abs/2507.08996. (accessed December 22, 2025).
(38) Culpitt, T.; Chen, Z.; Pavošević, F.; Yang, Y. Constrained Nuclear-Electronic Orbital Theory for Quantum Computation. *J. Chem. Theory Comput.* **2025**, *21*, 7845−7854.
(39) Li, Y.; Benjamin, S. C. Efficient Variational Quantum Simulator Incorporating Active Error Minimization. *Phys. Rev. X* **2017**, *7*, No. 021050.
(40) Temme, K.; Bravyi, S.; Gambetta, J. M. Error Mitigation for Short-Depth Quantum Circuits. *Phys. Rev. Lett.* **2017**, *119*, No. 180509.
(41) Bonet-Monroig, X.; Sagastizabal, R.; Singh, M.; O'Brien, T. E. Low-Cost Error Mitigation by Symmetry Verification. *Phys. Rev. A* **2018**, *98*, No. 062339.
(42) Huggins, W. J.; McArdle, S.; O'Brien, T. E.; Lee, J.; Rubin, N. C.; Boixo, S.; Whaley, K. B.; Babbush, R.; McClean, J. R. Virtual Distillation for Quantum Error Mitigation. *Phys. Rev. X* **2021**, *11*, No. 041036.
(43) McCaskey, A. J.; Parks, Z. P.; Jakowski, J.; Moore, S. V.; Morris, T. D.; Humble, T. S.; Pooser, R. C. Quantum Chemistry as a Benchmark for Near-Term Quantum Computers. *npj Quantum Inf.* **2019**, *5*, No. 99.

(44) Google AI Quantum and Collaborators; Arute, F.; Arya, K.; Babbush, R.; Bacon, D.; Bardin, J. C.; Barends, R.; Boixo, S.; Broughton, M.; Buckley, B. B.; Buell, D. A.; Burkett, B.; Bushnell, N.; Chen, Y.; Chen, Z.; Chiaro, B.; Collins, R.; Courtney, W.; Demura, S.; Dunsworth, A.; Farhi, E.; Fowler, A.; Foxen, B.; Gidney, C.; Giustina, M.; Graff, R.; Habegger, S.; Harrigan, M. P.; Ho, A.; Hong, S.; Huang, T.; Huggins, W. J.; Ioffe, L.; Isakov, S. V.; Jeffrey, E.; Jiang, Z.; Jones, C.; Kafri, D.; Kechedzhi, K.; Kelly, J.; Kim, S.; Klimov, P. V.; Korotkov, A.; Kostritsa, F.; Landhuis, D.; Laptev, P.; Lindmark, M.; Lucero, E.; Martin, O.; Martinis, J. M.; McClean, J. R.; McEwen, M.; Megrant, A.; Mi, X.; Mohseni, M.; Mruczkiewicz, W.; Mutus, J.; Naaman, O.; Neeley, M.; Neill, C.; Neven, H.; Niu, M. Y.; O'Brien, T. E.; Ostby, E.; Petukhov, A.; Putterman, H.; Quintana, C.; Roushan, P.; Rubin, N. C.; Sank, D.; Satzinger, K. J.; Smelyanskiy, V.; Strain, D.; Sung, K. J.; Szalay, M.; Takeshita, T. Y.; Vainsencher, A.; White, T.; Wiebe, N.; Yao, Z. J.; Yeh, P.; Zalcman, A. Hartree-Fock on a superconducting qubit quantum computer. *Science* **2020**, *369*, 1084−1089.
(45) Lolur, P.; Skogh, M.; Dobrautz, W.; Warren, C.; Biznárová, J.; Osman, A.; Tancredi, G.; Wendin, G.; Bylander, J.; Rahm, M. Reference-State Error Mitigation: A Strategy for High Accuracy Quantum Computation of Chemistry. *J. Chem. Theory Comput.* **2023**, *19*, 783−789.
(46) Saxena, G.; Kyaw, T. H. Error Mitigation by Restricted Evolution, arXiv:2409.06636. arXiv.org e-Print archive, 2024. https://arxiv.org/abs/2409.06636. (accessed December 22, 2025).
(47) Díez-Valle, P.; Saxena, G.; Baker, J. S.; Lee, J.-H.; Kyaw, T. H. Physics-Inspired Extrapolation for Efficient Error Mitigation and Hardware Certification, arXiv:2505.07977. arXiv.org e-Print archive, 2025 https://arxiv.org/abs/2505.07977. (accessed December 22, 2025).
(48) Bartlett, R. J.; Kucharski, S. A.; Noga, J. Alternative Coupled-Cluster Ansätze II. The Unitary Coupled-Cluster Method. *Chem. Phys. Lett.* **1989**, *155*, 133−140.
(49) Pavošević, F.; Hammes-Schiffer, S. Triple Electron−Electron−Proton Excitations and Second-Order Approximations in Nuclear−Electronic Orbital Coupled Cluster Methods. *J. Chem. Phys.* **2022**, *157*, No. 074104.
(50) Jordan, P.; Wigner, E. Über das Paulische Äquivalenzverbot. *Z. Phys.* **1928**, *47*, 631−651.
(51) Somma, R.; Ortiz, G.; Gubernatis, J. E.; Knill, E.; Laflamme, R. Simulating Physical Phenomena by Quantum Networks. *Phys. Rev. A* **2002**, *65*, No. 042323.
(52) Seeley, J. T.; Richard, M. J.; Love, P. J. The Bravyi-Kitaev Transformation for Quantum Computation of Electronic Structure. *J. Chem. Phys.* **2012**, *137*, No. 224109.
(53) McClean, J. R.; Rubin, N. C.; Sung, K. J.; Kivlichan, I. D.; Bonet-Monroig, X.; Cao, Y.; Dai, C.; Fried, E. S.; Gidney, C.; Gimby, B.; Gokhale, P.; Häner, T.; Hardikar, T.; Havlíček, V.; Higgott, O.; Huang, C.; Izaac, J.; Jiang, Z.; Liu, X.; McArdle, S.; Neeley, M.; O'Brien, T.; O'Gorman, B.; Ozfidan, I.; Radin, M. D.; Romero, J.; Sawaya, N. P. D.; Senjean, B.; Setia, K.; Sim, S.; Steiger, D. S.; Steudtner, M.; Sun, Q.; Sun, W.; Wang, D.; Zhang, F.; Babbush, R. OpenFermion: The Electronic Structure Package for Quantum Computers. *Quantum Sci. Technol.* **2020**, *5*, No. 034014.
(54) Treinish, M.; Lishman, J.; Bello, L.; Gambetta, J.; Rodríguez, D. M.; Marques, M.; Gacon, J.; Nation, P.; Wood, C. J.; ewinston; Gomez, J.; Chen, R.; Cross, A.; Krsulich, K.; Wood, S.; Ivrii, A.; Sertage, I. F.; Kanazawa, N.; Tapia, E. P.; Capelluto, L.; Alexander, T.; Arellano, E.; Hamamura, I.; Navarro, E.; Imamichi, T.; de la Puente González, S.; Thomas, S.; Sanchez, R.; Garion, S. Qiskit/qiskit: Qiskit 2.3.0rc1. 2025.
(55) Hehre, W. J.; Stewart, R. F.; Pople, J. A. Self-Consistent Molecular-Orbital Methods. I. Use of Gaussian Expansions of Slater-Type Atomic Orbitals. *J. Chem. Phys.* **1969**, *51*, 2657−2664.
(56) Ditchfield, R.; Hehre, W. J.; Pople, J. A. Self-Consistent Molecular-Orbital Methods. IX. An Extended Gaussian-Type Basis for Molecular-Orbital Studies of Organic Molecules. *J. Chem. Phys.* **1971**, *54*, 724−728.
(57) Grimsley, H. R.; Economou, S. E.; Barnes, E.; Mayhall, N. J. An Adaptive Variational Algorithm for Exact Molecular Simulations on a Quantum Computer. *Nat. Commun.* **2019**, *10*, No. 3007.
(58) Leymann, F.; Barzen, J. The Bitter Truth about Gate-Based Quantum Algorithms in the NISQ Era. *Quantum Sci. Technol.* **2020**, *5*, No. 044007.
(59) Motta, M.; Sung, K. J.; Whaley, K. B.; Head-Gordon, M.; Shee, J. Bridging Physical Intuition and Hardware Efficiency for Correlated Electronic States: The Local Unitary Cluster Jastrow Ansatz for Electronic Structure. *Chem. Sci.* **2023**, *14*, 11213−11227.

https://doi.org/10.1021/acs.jctc.5c01911
J. Chem. Theory Comput. 2026, 22, 1760−1769